

Crossbar Array of Artificial Synapses Based on Ferroelectric Diodes

Laura Seufert, Morteza Hassanpour Amiri, Paschalis Gkoupidenis, and Kamal Asadi*

Two terminal devices that exhibit resistance switching in response to an external voltage are interesting for neuromorphic computing applications. Owing to its simple device structure, a crossbar array of two-terminal resistance switching devices is highly desired for application as artificial neural network weights. Here, ferroelectric diodes that show resistance switching in their forward bias are presented. The resistance can be set to a high- and a low-resistance state or any state between these limits. It is demonstrated that the ferroelectric diodes can function as an artificial synapse. An array of the ferroelectric diodes with two bit and two row lines (2×2) is demonstrated. The resistance of every bit is independently tuned, and spike-time-dependent plasticity is shown for the array.


1. Introduction

Neuromorphic devices are being developed to emulate the information processing and memory functions of the human brain. The goal is to realize non-Von Neumann architecture for computing units, which enable massively parallel processing and save computing time and energy consumption.^[1–5] The strength of the connection between two artificial neurons is determined by synaptic weight, which is responsible for conveying the electrical signals between the two neurons. Artificial neurons have already been developed based on CMOS-based processors.^[6–9] However, their high energy consumption is still an issue that is yet to be addressed. An alternative approach is to use materials that inherently exhibit reversible switching in their electrical, magnetic, or optical property upon applying an electric field, magnetic field, or light.^[10–13]

L. Seufert, M. Hassanpour Amiri, P. Gkoupidenis, K. Asadi
Max Plank Institute for Polymer Research
Ackermannweg 10, 55128 Mainz, Germany

K. Asadi
Department of Physics
University of Bath
Claverton Down, Bath BA2 7AY, UK
E-mail: ka787@bath.ac.uk

K. Asadi
Centre for Therapeutic Innovation
University of Bath
Claverton Down, Bath BA2 7AY, UK

 The ORCID identification number(s) for the author(s) of this article can be found under <https://doi.org/10.1002/aelm.202100558>.

© 2021 The Authors. Advanced Electronic Materials published by Wiley-VCH GmbH. This is an open access article under the terms of the Creative Commons Attribution-NonCommercial License, which permits use, distribution and reproduction in any medium, provided the original work is properly cited and is not used for commercial purposes.

DOI: 10.1002/aelm.202100558

Memristors have emerged as a promising candidate for the realization of neuromorphic devices.^[14–18] The memristor's resistance can be tuned by applying a voltage in a nonvolatile but reversible fashion. The resistance changes between a high-resistance off-state and a low-resistance on-state, or any state in between these two limits. The programmed states are stable in time (typically years). Memristors usually operate based on filamentary conduction and have been realized in various metal oxides to polymeric-based systems. A 2D crossbar array of memristors, where the resistance-switching material is sandwiched between rows and columns of

electrodes and every crossing forms an individual memristor, is required for neuromorphic applications. However, a crossbar array of resistance-switching elements is prone to crosstalk which impedes reading of the resistance states of individual components. The issue can be addressed by using an active matrix addressing scheme at the expense of increased complexity.

An ideal resistance-switching device is a memory diode (memdiode), which is a rectifying diode that shows resistance switching and bistability only at forward bias. Unlike conventional memristors, the rectifying behavior of the memdiodes allows for the realization of a 2D array of such memdiodes without the need for auxiliary addressing or driving devices^[20–22] because such an array is immune against crosstalk.^[19,20]

Ferroelectrics have been extensively used in Boolean memory devices because of their bistable remanent polarization response upon application of (large enough) electric fields.^[23] Depending on the state of their remanent polarization, $+P_r$ or $-P_r$, digital 0 and 1 states can be programmed.^[24] Recently, the application of ferroelectrics in neuromorphic devices, particularly artificial synapses, has gained attention due to the possibility of setting their polarization state to any intermediate value between $-P_r$ and $+P_r$ limits. It is the time stability of the intermediate polarization states that makes ferroelectrics a strong contender.^[25,26] Ferroelectric synapses, along with their spike-timing-dependent plasticity (STDP), have been reported in ferroelectric field-effect transistors (FeFET)^[26–29] and ferroelectric tunnel junction (FTJ).^[30–32] Ferroelectric neurons have also been reported, which can enable adaptive learning functionality.^[33–35] Adaptation of ferroelectrics in neuromorphic devices has witnessed significant progress over the past decade, yet there are still a few challenges ahead.

The ferroelectric devices, i.e., capacitors, transistors, and tunnel junctions, that are used to realize the artificial neurons or synapses, face numerous challenges. For instance, capacitors have the simplest device form but cannot be used as synapses

because information readout requires accessing the (intermediate) polarization state, which is usually done by applying an external field and altering the polarization state. Hence, the readout is destructive, and restoring the polarization state is required after every readout operation. A second reference capacitor and an active-matrix scheme should be used to avoid information corruption, substantially increasing the complexity. The FeFETs resolve the destructive readout issue because their operation is based on the resistance switching of the FET channel, which stems from the modulation of the charge carrier density in the semiconductor channel by the polarization of the ferroelectric gate.^[36] However, the realization of 2D crossbar arrays of FeFET synapses is inherently impossible. For array realization for synaptic applications, two-terminal ferroelectric tunnel junction devices (FTJs) are ideal. In an FTJ, the ferroelectric layer is thin enough to allow for quantum mechanical tunneling of the electrons from the anode through the ferroelectric layer to the counter electrode.^[22,37,38] Despite their great promise, FTJs have mainly remained a research curiosity because contact formation on ultrathin ferroelectric films is very challenging.^[22] Direct deposition of metals onto ultrathin layers can easily create electrical shorts.^[39] Consequently, FTJs have been usually realized using scanning probe techniques, which suffer from poorly defined contact geometry, device area, and scalability.^[26,38,40] Recent demonstration of coplanar electrode geometry is a promising development toward the upscaled fabrication of FTJs.^[22,31]

Ferroelectric diodes^[41,42] are among the least explored devices for neuromorphic applications. Resistance switching at the forward bias has been realized for both inorganic ferroelectric Schottky diodes^[43] and organic ferroelectric diodes.^[19,44] The operation mechanism for both diodes is based on modulation of the injection barrier by the ferroelectric polarization. Both devices show robust memdiode behavior. However, arrays of synapses based on ferroelectric diodes remain to be demonstrated. Here, we present synaptic functionality in bistable rectifying ferroelectric diodes. The diodes have been realized with a phase-separated blend of ferroelectric polymer poly(vinylidene fluoride-co-trifluoroethylene), P(VDF-TrFE), with semiconducting polymer poly(9,9-dioctylfluorene) (PFO). The ferroelectric diodes are processed from the solution, and a 2D crossbar array architecture is realized.^[20,21,44–47] We show that the conductance of the diode for the forward bias can be reliably programmed to any intermediate states between the low resistance on-state and high-resistance off-state limits. It is shown that synaptic weight and spike-time dependent plasticity can be realized by programming the intermediate resistance states, which can be achieved by using a half-select scheme, i.e., applying 0.5 V over the word line and -0.5 V over the bit line, and varying the amplitude or width of the pre- and post-synaptic pulses. The resulting synaptic weight is stable in time. Finally, a 4-bit array of ferroelectric diodes is demonstrated wherein the resistance of each diode, hence its synaptic weight, is independently set.

2. Results and Discussion

P(VDF-TrFE) and PFO, chemical structures are given in Figure 1b, are co-dissolved in a common solvent,

tetrahydrofuran (THF) with 1:9 PFO:P(VDF-TrFE) weight ratio. Thin films are prepared from the blend solution. The blend film exhibits a phase-separated microstructure of vertical PFO domains in the P(VDF-TrFE) matrix, as schematically shown in Figure 1a. Atomic force microscopy (AFM) images of the thin films of PFO:P(VDF-TrFE) blends, Figure 1d, reveal randomly dispersed and isolated circular PFO domains in the semicrystalline P(VDF-TrFE) matrix. It is well-established that the PFO domains have mostly cylindrical structures, some continuous through the film thickness establishing a conduction path between the top and bottom electrodes. A small fraction of PFO domains do not contribute to current due to their discontinuity. A cross-sectional schematic of the device layout is given in Figure 1a. The current–voltage (I – V) characteristics of the diodes are presented in Figure 1e. At low biases, below the coercive field, the diode is highly resistive, and only a low current of about 0.1 nA passes through. When the bias reaches near 10 V, the current begins a sharp rise and at 15 V reaches values as high as 1 μ A. Hence, an increase of the order of 10^4 is achieved. The increase in current passing through the PFO phase is due to the polarization of the P(VDF-TrFE) matrix, as will be explained next.

The work function of the Au electrode is 4.7 eV, whereas the highest occupied molecular orbital (HOMO) of PFO is ≈ 5.9 eV. The barrier height for hole injection is considerable and amounts to 1.2 eV, efficiently blocking the injection of holes from the Au contact into the PFO, as shown in Figure 1c. Therefore, Au forms a Schottky barrier with the PFO phase for hole injection at the interfaces and is an injection-limited contact for hole injection into PFO. Next, a voltage is applied to the bottom Au electrode. At low positive biases, well below the coercive bias for polarization switching of P(VDF-TrFE), the current is low because of the significant injection barrier between the Au contact and the PFO phase. By increasing the applied positive bias, the P(VDF-TrFE) phase begins to polarize. The compensation charges in the Au electrode stabilize the polarization of the ferroelectric phase. On the other hand, these compensation charges create a stray field at the interface where the Au contact, PFO and P(VDF-TrFE) meet. At the coercive bias, the ferroelectric phase is fully polarized into its negative polarization state, where the polarization vector points away from the bottom Au electrode. The polarization compensation results in a sizeable stray field that penetrates the PFO phase, as shown with a yellow arrow in Figure 1a, facilitating the tunneling injection of holes by substantially reducing the barrier width. The injected holes effectively set the potential in the PFO phase equivalent to the Au contact, causing bending of the electric field lines and the appearance of an in-plane polarization component.^[48] The in-plane polarization is stabilized by the injected holes accumulated in the PFO phase alongside the interface with the P(VDF-TrFE) phase from the bottom Au electrode to the top electrode. The injected charges are transported through this channel from the anode to the cathode, as shown with the blue arrow in Figure 1a. Consequently, the barrier is effectively removed, and the resistance of the diode in the forward bias shows a sharp rise from the high-resistance off-state to the low-resistance on-state. When the bias is lowered towards 0 V, the resistance remains low, and the current passing through the device stays high, and the diode shows bistability in its

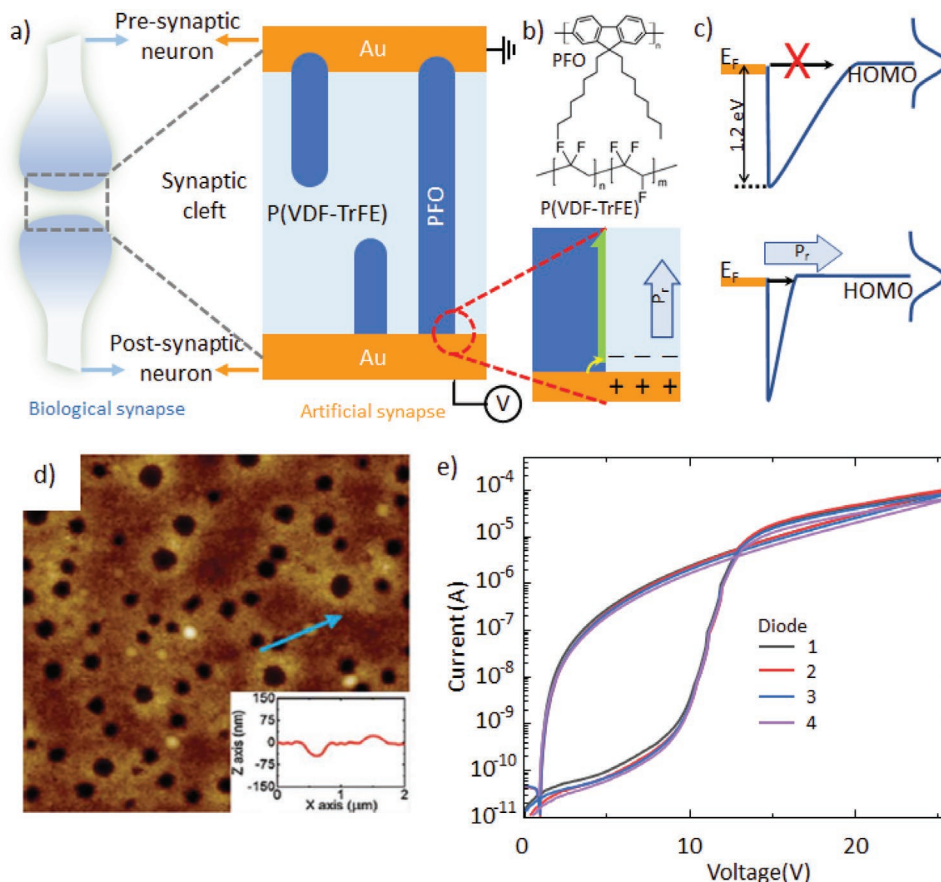


Figure 1. a) A schematic representation of a biological synapse and a ferroelectric diode synapse. The dashed gray line shows the similarity of the PFO:P(VDF-TrFE) to a synaptic cleft. The dashed red line highlights the significance of the interface between the Au electrode, PFO, and P(VDF-TrFE), where the compensation of ferroelectric polarization yields a strong stray field (yellow arrow) leading to efficient hole injection and transport (blue arrow). b) The chemical structures of PFO and P(VDF-TrFE) and the red . c) Band diagram at the Au/PFO contact for the polarized (top) and negatively polarized (bottom) P(VDF-TrFE) phase. d) A typical AFM image of the morphology of the PFO:P(VDF-TrFE) film. The inset shows the height profile of the surface along the arrow. e) Individual I - V characteristic curves of four ferroelectric diodes on a 2×2 array.

resistance in the forward bias. When the bias becomes negative, the diodes remain nonconductive and rectifying for biases below the negative coercive bias. Polarization switches direction for the negative biases higher than the negative coercive bias, and the P(VDF-TrFE) phase becomes positively polarized with the polarization vector pointing toward the bottom Au electrode. The change of polarization reverses the direction of the stray field, reestablishing the injection barrier at the interface and setting the diode back to its off state.^[48]

The ferroelectric diode can be used as an artificial synapse, as schematically shown in Figure 1a, where the Au contacts represent pre- and post-synaptic neurons and the phase-separated PFO:P(VDF-TrFE) film can be considered as a synaptic cleft. In the following, it is shown how the ferroelectric diode can function as a synapse.

To function as a synapse, gradual and nonvolatile change of the diode's conductance is crucial. The conductance change depends on the polarization state of the ferroelectric phase. Polarization switching of the ferroelectric strongly depends on the amplitude and width of the external pulse.^[49] Hence, the switching time of the memory diode is not a unique value as it is determined by both width and amplitude of the applied

pulse. In the next step, the polarization of the ferroelectric phase is controlled by changing the amplitude of the switching pulse while keeping the pulse width constant. **Figure 2a** unambiguously demonstrates a gradual change of the conductance and that the diode can be set in any intermediate resistance state. As an example, six different intermediate states are programmed between the high- and low-resistance states. Interestingly, partial polarizations of the ferroelectric phase, which yield intermediate resistance states, are stable in time, and the resistance of the programmed intermediate states shows stability in time for over 1500 s, as presented in Figure 2b. We note that the suitability of the ferroelectric diodes for neuromorphic applications has been discussed in our recent review.^[19] However, the provided examples lack polarization stability, which is the basic necessity for neuromorphic applications. To stabilize the ferroelectric polarization, the depolarization field should be nullified by using contacts that are ambipolar semiconductors or metals. Otherwise, the ferroelectric phase depolarizes rapidly, and the diode loses its information state in time (in much less than a second, as shall be discussed later).^[57]

Resistance switching of the ferroelectric diode depends on the temporal behavior of the ferroelectric polarization and is

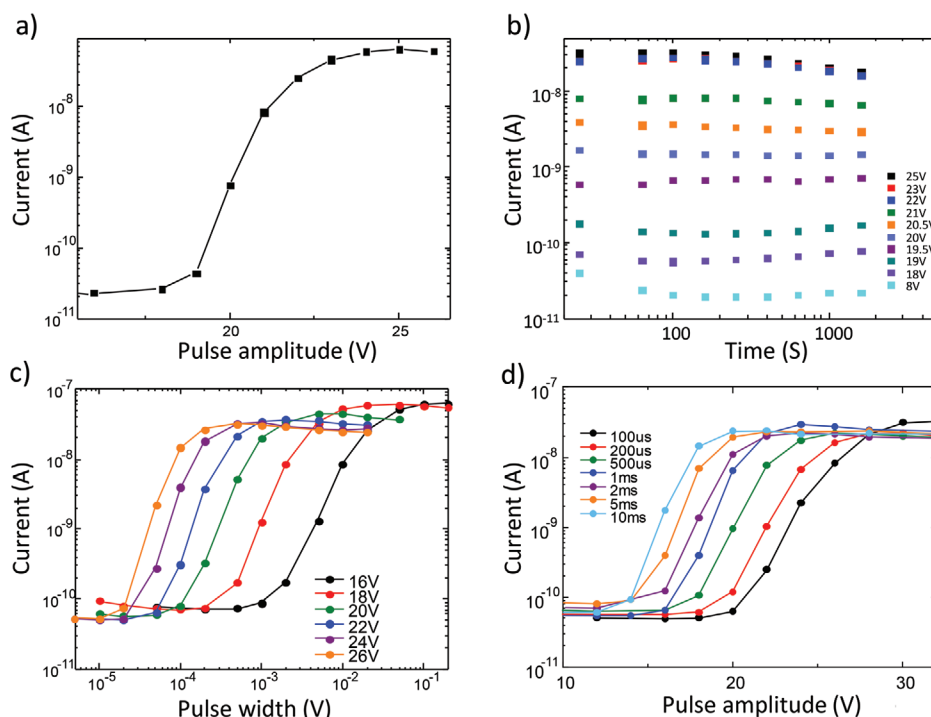


Figure 2. a) Gradual increase of the conductance of the ferroelectric diode by increasing the amplitude of the writing pulses from 15 to 26 V at a constant reading pulse amplitude of 5 V. Intermediate states can be programmed by changing the amplitude of the applied bias. b) Retention of the programmed resistance state for various writing pulse amplitudes with 500 μ s pulse width. c,d) Programming of the intermediate states using pulses of different amplitudes (fixed pulse width) and various pulse width (with fixed amplitude), respectively. Read voltage in all cases is +5 V.

determined by both the amplitude and duration of the applied pulse. Knowledge of the pulse width and amplitude leading to a threshold behavior is of practical importance for later realizing ferroelectric diodes with a transition between short- and long-term memory phenomena. To that end, both the width and amplitude of the programming pulses are changed in the next step to demonstrate the programmability of the diodes using different pulsing scenarios. Figure 2c shows that the coercive field initializing the switching of ferroelectric polarization depends on the pulse amplitude. For a larger amplitude, the programming time of the diode is shorter. However, the number of intermediate states that can be programmed reliably decreases.

Nevertheless, the possible values of the high- and low-resistance states are independent of the pulsing conditions. It should be noted that the energy required for the programming of the diode from the off- to the on-state using 26 V pulses can be as low as 25 nJ. Moreover, regardless of the pulsing conditions, the programmed intermediate conductance states are stable in time, as demonstrated in Figure 2b. A similar switching behavior can be observed when the pulse width is varied (for a fixed amplitude), as presented in Figure 2d. For longer pulse amplitude, change of conductance begins at smaller voltages. Therefore, the resistance of discrete ferroelectric diodes can be reliably and controllably changed by several orders of magnitude between a high- and a low-resistance state.

The ferroelectric diode has an asymmetric structure. Therefore, similar but mirrored on-to-off and off-to-on current transitions are intuitively expected. The switching of polarization

depends on two factors, pulse amplitude and pulse width. To unambiguously show the effect of pulse amplitude, we fixed the pulse width to 500 μ s and applied pulses of variable amplitude to the device. As shown in Figure 3a, the device shows both clear transitions from off-to-on (LTP) for positive pulses and a mirror-imaged transition from on-to-off (LTD) for negative switching pulses. There is a subthreshold regime that depends on the pulsing conditions, as can be seen in Figure 2c,d. When the diode is biased in the subthreshold regime, i.e., by applying voltages lower than the coercive voltage, the ferroelectric phase polarizes. However, the polarization is unstable/volatile and not retained after the voltage goes back to zero.

Depolarization of the ferroelectric can therefore enable to realize short-term memory effects in the diodes. To that end, we determine the paired-pulse facilitation (PPF) index by applying two consecutive pulses with a varying time interval between the pulses. The second pulse can cause an enhanced response in post-synaptic current PPF yielding short-term synaptic plasticity. In biological systems, the PPF enhances for a reduced time interval between paired pulses. The PPF percentage, defined as the $100 \times (I_2 - I_1)/I_1$, usually follows a double-exponential equation $PPF = C_1 \times \exp(-\Delta t/\tau_1) + C_2 \times \exp(-\Delta t/\tau_2)$, where Δt is the time interval between the pulses, C_1 and C_2 are the PPF indexes of two phases, and τ_1 and τ_2 are the characteristic relaxation times, respectively. The diode set in the off-state is subjected to repeated pulses of fixed amplitude and width of, respectively, 14 V and 5 ms to demonstrate the programming characteristics. The time interval between the two pulses is varied from 2 μ s to 5 ms. The choice of amplitude and width

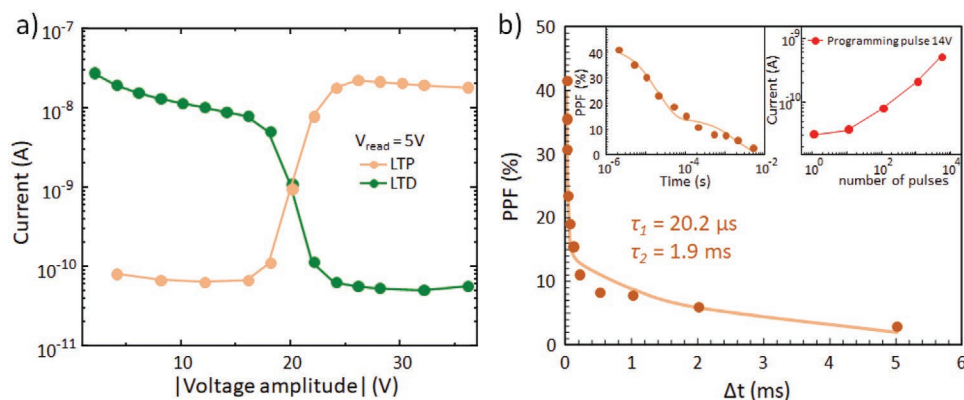


Figure 3. a) Current transition for off-to-on (LTP) and on-to-off (LTD) for P(VDF-TrFE):PFO diode, by applying pulses with a fixed width of 500 μ s and variable amplitude of -2 to -36 V for LTD and $+4$ to $+36$ V for LTP. b) Paired-pulse facilitation in ferroelectric diodes using pulses with a fix amplitude and width of 14 V and 5 ms, respectively. The left inset shows PPF on logarithmic time axis. The right inset shows programming characteristics of the ferroelectric diodes after repeated pulsing. Read voltage in both cases is $+5$ V.

of the switching pulses is determined from the experimental conditions, as demonstrated in Figure 2c,d, to allow for a sub-threshold behavior. Measured PPF index as a function of Δt is given in Figure 3b. Fitting the PPF data using a double exponential function produces the following values for $C_1 = 28.7\%$, $C_2 = 14.1\%$, $\tau_1 = 20.2 \mu$ s, and $\tau_2 = 2.0$ ms. The maximum PPF index at $\Delta t = 0$, corresponding to the situation of two input stimuli firing together to a synapse, is given by $C_1 + C_2 = 42.8\%$. As shown, the PPF shows a sharp drop, particularly for time intervals below 100 μ s (inset Figure 3b).

The PPF results can be explained based on the polarization switching mechanism in ferroelectric polymers.^[58] Applying a bias just below the coercive bias results in the nucleation of isolated domains with reversed polarization. However, after removing the bias, the nucleated domain cannot retain its polarization state as it requires energy. Therefore, the domain loses its reversed polarization and goes back to its original polarization state. Application of a second pulse can prevent reversal of the polarization for the nucleated domains, provided that the time interval between the first and second pulse is shorter than the polarization relaxation dynamics. For ferroelectric polymers, the polarization time of the nucleated domains is in the order of tens of μ s,^[58] depending on the pulsing conditions. Therefore, the value obtained for $\tau_1 = 20.2 \mu$ s corresponds to polarization dynamic of the ferroelectric phase and matches closely the experimental values obtained in Figure 2c, indicating an internal consistency of the measurements. Therefore, for Δt values shorter than $\tau_1 = 20.2 \mu$ s, a larger PPF index is expected. As Δt increases beyond τ_1 , the depolarization dynamic prevails, and the PPF index drops substantially. We note that an exponential drop in the PPF index is expected because polarization dynamics follows an exponential.

After establishing the depolarization dynamic with the PPF measurement, it is possible to obtain long-term plasticity using similar repeated pulsing conditions. To that end, the diode set in the off-state is subjected to repeated pulses of fixed amplitude and width of respectively 14 V and 5 ms (similar to those used for PPF). The timing interval between the pulses is set to 10 μ s. The resistance of the diode is measured after several pulses were applied. As presented in the inset of Figure 3b,

the current passing through the diode at $+5$ V shows a gradual increase upon repeated pulsing. The measurement indicates that a stable state is achieved after the application of at least ten pulses. Hence, the resistance of the diodes can be gradually switched using repeated pulses just below the coercive bias. We note that this finding agrees with previous reports on complete polarization reversal in ferroelectrics by repeated voltage pulses with an amplitude that is just below the coercive bias.^[55] Furthermore, it should be noted that the current after 10^4 pulses is slightly lower than that of the on-state current level for a fresh diode due to the fatigue of the P(VDF-TrFE) polymer, which usually appears after 1000 pulses if specific pulsing conditions are not met.^[55]

The PFO:P(VDF-TrFE) diode can be used as an artificial synapse to emulate signal propagation between two neighboring neurons, as shown in Figure 1a. To be suited for neuromorphic computing, parallel programming and readout of artificial neural network weights in a crossbar memory array is needed.^[50] To that end, a 2×2 array of PFO:P(VDF-TrFE) diodes is fabricated. A schematic of the array is given in Figure 4a. To program a bit, as discussed elsewhere and in the Experimental Section,^[20] a half voltage scheme is used on the word- and bit-lines while other word- and bit-lines are grounded.^[20,21] As shown in Figure 4a, the resistance of each bit can be very well controlled. The suitability of the array of ferroelectric diodes for neural network weight is demonstrated through STDP of the diodes. The STDP is a widely studied mechanism for regulating neural activities, predominantly focusing on the relative firing time in the pre- and post-synapses.^[51–53] The pre- and post-pulses are applied on the Au top and bottom electrodes, respectively. The timing between the two pulses is systematically varied from 0 to 1 s. The pulsing strategy to induce STDP is given in Figure 4b. The amplitude of the pre-spike pulse is positive and is below the coercive field. When the post-spike pulse (-10 V, 500 μ s) overlaps with the pre-spike pulse, the total potential will be above the coercive bias, and the polarization state will change depending on the overlapping time. By choosing the pre-spike pulse amplitudes as shown in Figure 4b, it is shown that the polarization state of the ferroelectric phase depends on the timing between the two pulses, in the same way as the

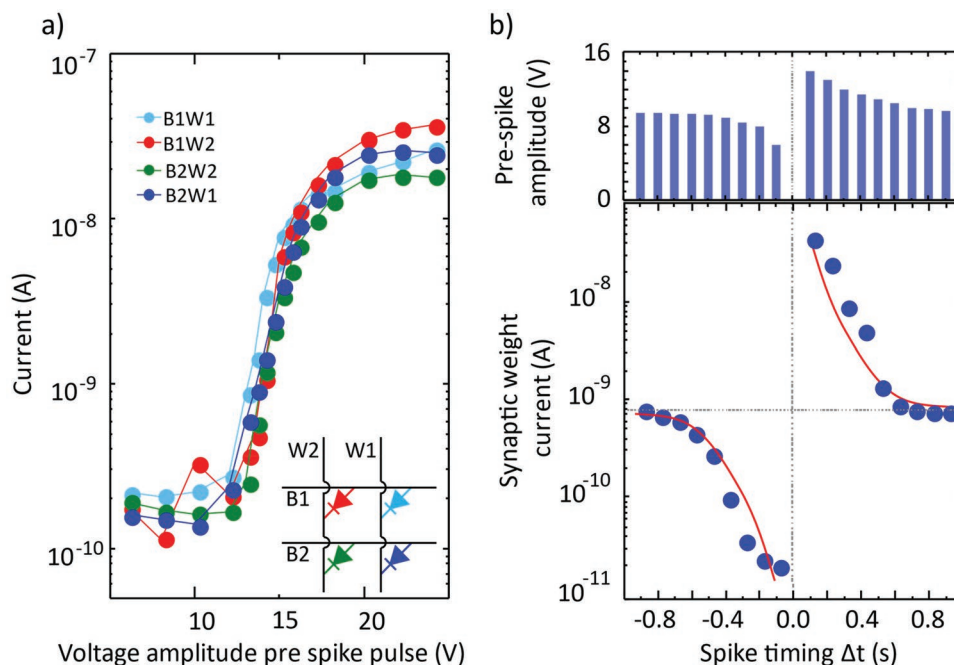


Figure 4. a) Demonstration of a 2×2 , 4-bit crossbar array of ferroelectric diodes (inset) with programming intermediate resistance stated in every bit. b) Demonstration of spike-timing dependent plasticity for the ferroelectric diode artificial synapse. The red solid line is a guide to the eye. The top bar graph shows the pre-spike pulse train that is applied to the bit lines. Note that the voltage is positive. The post-synaptic pulse is -10 V and is applied to the word lines. The pulse width is $500 \mu\text{s}$ and the read voltage is $+5$ V.

synaptic weight. For the post pulse being slightly earlier or later than the time reference point, labeled by “0” on the time axis in Figure 4b, there will be maximum depression and potentiation. Achieving STDP behavior, as shown in Figure 4b, indicates that ferroelectric diodes can be used as artificial synapses. Firing post-spike pulses before pre-spike pulses results in a decreasing trend in the read current known as long-term depression (LTD), whereas a reversal in the temporal order of the pre- and post-pulses induces a long-term potentiation (LTP).^[54]

3. Conclusion

It is demonstrated that ferroelectric diodes realized with phase-separated blends of organic semiconductor (PFO) and a ferroelectric polymer (P(VDF-TrFE)) can function as artificial synapses for application in artificial neural networks. Multistate resistance switching and various synaptic functionalities such as STDP, LTP, LTD, and PPF have been successfully demonstrated in a 2×2 array of ferroelectric diodes. As the present study focuses on demonstrating the feasibility of the ferroelectric diodes for neuromorphic applications, little attention is paid to optimizing the devices for low voltage operations. Nevertheless, low voltage operation (sub-5 V) has already been demonstrated for the memory diodes.^[45,56] Furthermore, previous demonstrations of air-stable^[22] and 1 kb crossbar arrays of ferroelectric diodes as memory elements^[21] highlight the great potential of ferroelectric diodes for neuromorphic applications. However, the previous works^[21,22] have been only focused on arrays of binary memories, without any ramification on synaptic electronics.

4. Experimental Section

Random copolymer P(VDF-TrFE) with the molar composition of 75% VDF and 35% TrFE was purchased from Solvay and used as received. PFO was synthesized in-house using previously reported procedures. To fabricate the ferroelectric diodes, P(VDF-TrFE) and PFO were co-dissolved in a common solvent, THF. The solution was then spin-coated onto a cleaned glass slide with pre-deposited Cr/Au bottom electrodes (1 nm/50 nm). The process was done under a nitrogen atmosphere inside a glove box.

The film thickness was tuned between 212 ± 16 and 258 ± 5 nm, depending on the spinning speed. Afterward, the substrates were annealed at 140°C for 90 min in a vacuum oven. The diodes were finished by deposition of a 50 nm gold top contact. Both bottom and top contacts were realized through shadow mask evaporation. The crossbar arrays were fabricated by shadow masks deposition of Cr/Au lines (1 nm/50 nm) as bottom electrodes. After deposition and annealing of the blend film, counter electrodes were deposited through the same set of shadow masks, but by rotating the masks by 90° with respect to the bottom electrode lines. The area of the diodes, both individual devices and those in the array, was the same and amounted to 0.16 mm^2 . All electrical measurements were carried out using a Keithley 4200 SCS, equipped with a pulse measure unit, under a vacuum of 10^{-6} mbar and dark conditions to avoid oxygen contamination and photogenerated carrier. To program different bits in the array, $+0.5$ V was applied to the bit line, and the other -0.5 V was applied to the word line to make up full V over the selected bit. All the other bits and word lines were grounded. The same reading scheme was also used to readout the states.

Acknowledgements

L.S. and M.H.A. contributed equally to this work. The authors would like to thank Prof. Paul W. M. Blom and Dr. M. Kumar for fruitful discussions, C. Bauer and F. Keller for technical assistance, and M. Beuchel for the synthesis of PFO. This work received financial

support from the Alexander von Humboldt Foundation and Max Planck Institute for Polymer Research.

Open access funding enabled and organized by Projekt DEAL.

Conflict of Interest

The authors declare no conflict of interest.

Data Availability Statement

The data that support the findings of this study are available from the corresponding author upon reasonable request.

Keywords

array, ferroelectric diode, memristor, plasticity, synapse

Received: May 27, 2021

Revised: September 14, 2021

Published online: October 15, 2021

- [1] W. Zhang, B. Gao, J. Tang, P. Yao, S. Yu, M.-F. Chang, H.-J. Yoo, H. Qian, H. Wu, *Nat. Electron.* **2020**, *3*, 371.
- [2] S. Bains, *Nat. Electron.* **2020**, *3*, 348.
- [3] D. S. Jeong, K. M. Kim, S. Kim, B. J. Choi, C. S. Hwang, *Adv. Electron. Mater.* **2016**, *2*, 1600090.
- [4] D. Kuzum, S. Yu, H.-S. P. Wong, *Nanotechnology* **2013**, *24*, 382001.
- [5] M. Hu, C. E. Graves, C. Li, Y. Li, N. Ge, E. Montgomery, N. Davila, H. Jiang, R. S. Williams, J. J. Yang, Q. Xia, J. P. Strachan, *Adv. Mater.* **2018**, *30*, 1705914.
- [6] G. Indiveri, B. Linares-Barranco, T. Hamilton, A. van Schaik, R. Etienne-Cummings, T. Delbruck, S.-C. Liu, P. Dudek, P. Häfliger, S. Renaud, J. Schemmel, G. Cauwenberghs, J. Arthur, K. Hynna, F. Folowosele, S. Saighi, T. Serrano-Gotarredona, J. Wijekoon, Y. Wang, K. Boahen, *Front. Neurosci.* **2011**, *5*, 73.
- [7] B. V. Benjamin, P. Gao, E. McQuinn, S. Choudhary, A. R. Chandrasekaran, J.-M. Bussat, R. Alvarez-Icaza, J. V. Arthur, P. A. Merolla, K. Boahen, *Proc. IEEE* **2014**, *102*, 699.
- [8] Q.-F. Ou, B.-S. Xiong, L. Yu, J. Wen, L. Wang, Y. Tong, *Materials* **2020**, *13*, 3532.
- [9] S. Bavikadi, P. R. Sutradhar, K. N. Khasawneh, A. Ganguly, S. M. P. Dinakarrao, in *Proc. 2020 GT Lakes Symp. VLSI*, Association for Computing Machinery, New York **2020**, pp. 89–94.
- [10] J. Grollier, D. Querlioz, K. Y. Camsari, K. Everschor-Sitte, S. Fukami, M. D. Stiles, *Nat. Electron.* **2020**, *3*, 360.
- [11] S. I. Kiselev, J. C. Sankey, I. N. Krivorotov, N. C. Emley, R. J. Schoelkopf, R. A. Buhrman, D. C. Ralph, *Nature* **2003**, *425*, 380.
- [12] M. Wuttig, H. Bhaskaran, T. Taubner, *Nat. Photonics* **2017**, *11*, 465.
- [13] D. Marković, A. Mizrahi, D. Querlioz, J. Grollier, *Nat. Rev. Phys.* **2020**, *2*, 499.
- [14] M. Xu, X. Mai, J. Lin, W. Zhang, Y. Li, Y. He, H. Tong, X. Hou, P. Zhou, X. Miao, *Adv. Funct. Mater.* **2020**, *30*, 2003419.
- [15] S. Fabiano, N. Sani, J. Kawahara, L. Kergoat, J. Nissa, I. Engquist, X. Crispin, M. Berggren, *Sci. Adv.* **2017**, *3*, e1700345.
- [16] K. M. Kim, B. J. Choi, Y. C. Shin, S. Choi, C. S. Hwang, *Appl. Phys. Lett.* **2007**, *91*, 012907.
- [17] D.-H. Kwon, K. M. Kim, J. H. Jang, J. M. Jeon, M. H. Lee, G. H. Kim, X.-S. Li, G.-S. Park, B. Lee, S. Han, M. Kim, C. S. Hwang, *Nat. Nanotechnol.* **2010**, *5*, 148.
- [18] H. Wang, X. Yan, S. Wang, N. Lu, *ACS Appl. Mater. Interfaces* **2021**, *13*, 17844.
- [19] K. Asadi, *Appl. Phys. Rev.* **2020**, *7*, 021307.
- [20] K. Asadi, M. Li, N. Stingelin, P. W. M. Blom, D. M. de Leeuw, *Appl. Phys. Lett.* **2010**, *97*, 193308.
- [21] A. J. J. M. van Breemen, J.-L. van der Steen, G. van Heck, R. Wang, V. Khikhlovskiy, M. Kemerink, G. H. Gelinck, *Appl. Phys. Express* **2014**, *7*, 031602.
- [22] M. Kumar, H. S. Dehsari, S. Anwar, K. Asadi, *Appl. Phys. Lett.* **2018**, *112*, 123302.
- [23] R. C. G. Naber, K. Asadi, P. W. M. Blom, D. M. De Leeuw, B. De Boer, *Adv. Mater.* **2010**, *22*, 933.
- [24] M. H. Amiri, J. Heidler, K. Müllen, K. Asadi, *ACS Appl. Electron. Mater.* **2020**, *2*, 2.
- [25] D. Zhao, I. Katsouras, K. Asadi, W. A. Groen, P. W. M. Blom, D. M. de Leeuw, *Appl. Phys. Lett.* **2016**, *108*, 232907.
- [26] S. Oh, H. Hwang, I. K. Yoo, *APL Mater.* **2019**, *7*, 091109.
- [27] M. H. Amiri, J. Heidler, K. Müllen, P. Gkoupidenis, K. Asadi, *Adv. Funct. Mater.* **2020**, *30*, 2003085.
- [28] L. Wang, W. Liao, S. L. Wong, Z. G. Yu, S. Li, Y.-F. Lim, X. Feng, W. C. Tan, X. Huang, L. Chen, L. Liu, J. Chen, X. Gong, C. Zhu, X. Liu, Y.-W. Zhang, D. Chi, K.-W. Ang, *Adv. Funct. Mater.* **2019**, *29*, 1901106.
- [29] S. Dai, Y. Zhao, Y. Wang, J. Zhang, L. Fang, S. Jin, Y. Shao, J. Huang, *Adv. Funct. Mater.* **2019**, *29*, 1903700.
- [30] S. Majumdar, H. Tan, Q. H. Qin, S. van Dijken, *Adv. Electron. Mater.* **2019**, *5*, 1800795.
- [31] M. Kumar, D. G. Georgiadou, A. Seitekhan, K. Loganathan, E. Yengel, H. Faber, D. Naphade, A. Basu, T. D. Anthopoulos, K. Asadi, *Adv. Electron. Mater.* **2020**, *6*, 1901091.
- [32] R. Guo, Y. Zhou, L. Wu, Z. Wang, Z. Lim, X. Yan, W. Lin, H. Wang, H. Y. Yoong, S. Chen, Ariando, T. V. , J. Wang, G. M. Chow, A. Gruverman, X. Miao, Y. Zhu, J. Chen, *ACS Appl. Mater. Interfaces* **2018**, *10*, 12862.
- [33] S. Yoon, E. Tokumitsu, H. Ishiwara, *IEEE Trans. Electron Devices* **2000**, *47*, 1630.
- [34] H. Ishiwara, Y. Aoyama, S. Okada, C. Shimamura, E. Tokumitsu, *Comput. Electr. Eng.* **1997**, *23*, 431.
- [35] Y. Nishitani, Y. Kaneko, M. Ueda, T. Morie, E. Fujii, *J. Appl. Phys.* **2012**, *111*, 124108.
- [36] K. Asadi, P. W. M. Blom, D. M. de Leeuw, *Appl. Phys. Lett.* **2011**, *99*, 053306.
- [37] A. Chanthbouala, V. Garcia, R. O. Cherifi, K. Bouzehouane, S. Fusil, X. Moya, S. Xavier, H. Yamada, C. Deranlot, N. D. Mathur, M. Bibes, A. Barthélémy, J. Grollier, *Nat. Mater.* **2012**, *11*, 860.
- [38] A. Gruverman, D. Wu, H. Lu, Y. Wang, H. W. Jang, C. M. Folkman, M. Y. Zhuravlev, D. Felker, M. Rzechowski, C.-B. Eom, E. Y. Tsymlal, *Nano Lett.* **2009**, *9*, 3539.
- [39] Y. Wang, M. K. Niranjan, K. Janicka, J. P. Velev, M. Y. Zhuravlev, S. S. Jaswal, E. Y. Tsymlal, *Phys. Rev. B* **2010**, *82*, 94114.
- [40] V. Garcia, S. Fusil, K. Bouzehouane, S. Enouz-Vedrenne, N. D. Mathur, A. Barthélémy, M. Bibes, *Nature* **2009**, *460*, 81.
- [41] T. Choi, S. Lee, Y. J. Choi, V. Kiryukhin, S.-W. Cheong, *Science* **2009**, *324*, 63 LP.
- [42] A. Q. Jiang, C. Wang, K. J. Jin, X. B. Liu, J. F. Scott, C. S. Hwang, T. A. Tang, H. Bin Lu, G. Z. Yang, *Adv. Mater.* **2011**, *23*, 1277.
- [43] P. W. M. Blom, R. M. Wolf, J. F. M. Cillessen, M. P. C. M. Krijn, *Phys. Rev. Lett.* **1994**, *73*, 2107.
- [44] K. Asadi, D. M. de Leeuw, B. de Boer, P. W. M. Blom, *Nat. Mater.* **2008**, *7*, 547.
- [45] M. Li, N. Stingelin, J. J. Michels, M.-J. Spijkman, K. Asadi, R. Beerends, F. Biscarini, P. W. M. Blom, D. M. de Leeuw, *Adv. Funct. Mater.* **2012**, *22*, 2750.
- [46] J. J. Michels, A. J. J. M. van Breemen, K. Usman, G. H. Gelinck, *J. Polym. Sci., Part B: Polym. Phys.* **2011**, *49*, 1255.

- [47] C. R. McNeill, K. Asadi, B. Watts, P. W. M. Blom, D. M. de Leeuw, *Small* **2010**, *6*, 508.
- [48] M. Ghittorelli, T. Lenz, H. S. Dehsari, D. Zhao, K. Asadi, P. W. M. Blom, Z. M. Kovács-Vajna, D. M. de Leeuw, F. Torricelli, *Nat. Commun.* **2017**, *8*, 15741.
- [49] K. Asadi, T. G. de Boer, P. W. M. Blom, D. M. de Leeuw, *Adv. Funct. Mater.* **2009**, *19*, 3173.
- [50] E. J. Fuller, S. T. Keene, A. Melianas, Z. Wang, S. Agarwal, Y. Li, Y. Tuchman, C. D. James, M. J. Marinella, J. J. Yang, A. Salleo, A. A. Talin, *Science* **2019**, *364*, 570 LP.
- [51] L. F. Abbott, S. B. Nelson, *Nat. Neurosci.* **2000**, *3*, 1178.
- [52] V. Egger, D. Feldmeyer, B. Sakmann, *Nat. Neurosci.* **1999**, *2*, 1098.
- [53] B. Gustafsson, H. Wigstrom, W. C. Abraham, Y. Y. Huang, *J. Neurosci.* **1987**, *7*, 774 LP.
- [54] Z. Wang, S. Joshi, S. E. Savel'ev, H. Jiang, R. Midya, P. Lin, M. Hu, N. Ge, J. P. Strachan, Z. Li, Q. Wu, M. Barnell, G.-L. Li, H. L. Xin, R. S. Williams, Q. Xia, J. J. Yang, *Nat. Mater.* **2017**, *16*, 101.
- [55] D. Zhao, I. Katsouras, M. Li, K. Asadi, J. Tsurumi, G. Glasser, J. Takeya, P. W. M. Blom, D. M. de Leeuw, *Sci. Rep.* **2014**, *4*, 5075.
- [56] M. Li, I. Katsouras, K. Asadi, P. W. M. Blom, D. M. de Leeuw, *Appl. Phys. Lett.* **2013**, *103*, 072903.
- [57] K. Asadi, J. Wildeman, P. W. M. Blom, D. M. de Leeuw, *IEEE Trans. Electron Devices* **2010**, *57*, 3466.
- [58] D. Zhao, I. Katsouras, K. Asadi, P. W. M. Blom, D. M. de Leeuw, *Phys. Rev. B* **2015**, *92*, 214115.